ISSN 0915-633X

NATIONAL INSTITUTE FOR FUSION SCIENCE

Coupling of Tilting Gaussian Beam with Hybrid Mode in the Corrugated Waveguide

K. Ohkubo, S. Kubo, H. Idei, M. Sato,
T. Shimozuma and Y. Takita

(Received - Nov. 27, 1996)

NIFS-474 Jan. 1997

RESEARCH REPORT
NIFS Series

NAGOYA, JAPAN

COUPLING OF TILTING GAUSSIAN BEAM WITH HYBRID MODE IN THE CORRUGATED WAVEGUIDE

K. Ohkubo, S. Kubo, H. Idei,
M. Sato, T. Shimozuma and Y. Takita

National Institute for Fusion Science,
Furo-cho, Chikusa-ku, Nagoya, 461-01, Japan

Abstract

The mode-conversion loss in the matching between the gaussian beam emanated from the gyrotron and the hybrid mode in the circular corrugated waveguide with the diameter of $2a$ is discussed. By numerical calculation, it is found that the loss considerably increases and optimum waist size w_0 changes when TEM_{00} mode with the wavelength λ is injected with offset or tilt. By fitting numerical data to the polynomial function, it becomes evident that the scaling formulas of the losses for the off-axis shift r_d and for the tilt angle θ are derived to be $2.3(r_d/a)^2 - 2.2(r_d/a)^4$ and $3.9(a\theta/\lambda)^2 - 5.6(a\theta/\lambda)^4$ for fixed w_0/a=0.643, respectively. To keep the mode-conversion loss $\leq$1% for the frequency of 168 GHz and $2a$=88.9 mm, tilting angle and offset should be less than 0.1 degrees and 2.9 mm, respectively.

Keywords: guassian beam, hybrid mode, HE_{11} mode, corrugated wave guide, coupling, gyrotron, electron cyclotron heating

Submitted to International Journal of Infrared and Milimeter Waves

1 Introduction

Recently, there has been an interest in electron cyclotron heating (ECH) of high temperature plasmas by high-power millimeter waves. To transmit efficiently the millimeter wave from a gyrotron, it is necessary to suppress a mode-conversion caused by offset and tilt in alignment of transmission system. Since the HE_{11} mode in the circular corrugated (CC) waveguide has advantages of low transmission loss [1], linear polarization and axisymmetry, the HE_{11} mode has been adopted as highly reliable transmission mode of millimeter waves [2, 3, 4]. The mode-conversion loss to the HE_{21} and TE_{01} modes for H-plane (or HE_{21} and TM_{02} modes for E-plane) [5] at the junction of the CC-waveguide with tilt θ is given by $2.2(a\theta/\lambda)^2$, respectively, where $2a$ is the waveguide diameter and λ is the wavelength in free space. Thus total loss of HE_{11} due to the higher mode-conversion is $4.4(a\theta/\lambda)^2$. For instance, in the HE_{11} mode transmission with the frequency of $\omega/2\pi$=170 GHz by means of the CC-waveguide with $2a$ = 88.9 mm, waveguide tilting of 3 mrad gives the total mode-conversion loss of 2%. As for an axial offset between waveguides r_d, the mode-conversion loss for the HE_{21} and TE_{01} modes for H-plane (or HE_{21} and TM_{02} modes for E-plane) [5] is written by $1.1(r_d/a)^2$, respectively. The total loss $2.2(r_d/a)^2$, for $r_d/a \sim 0.02$ is as small as 0.8%.

Experimental [3, 4] and theoretical [6, 7] studies on the coupling between a gaussian beam TEM_{00} from a gyrotron with a Vlasov converter and a hybrid mode HE_{11} in the CC-waveguide have been carried out. The results indicate that 98 % power of a incident beam can be coupled to the HE_{11} mode and that a part of remaining power propagates as an higher mode of HE_{12} in the waveguide and the other spills outside the waveguide. When a gaussian beam is injected to the CC-waveguide, offset and tilt as well as waist parameters affect strongly the coupling efficiency. By using the mode matching method, we analyze the effect of offset and tilt on the coupling efficiencies between a gaussian beam and hybrid modes.

This paper presents the evidence from the numerical calculation that TEM_{00}-to-HE_{11} mode power coupling efficiency strongly decreases with the incident angle and offset. The scaling laws on frequency and diameter of waveguide are shown for designing the matching optics unit between the gyrotron and transmission line in ECH system. The paper consists of four sections. In section 2, the electromagnetic (EM) fields of gaussian beam and hybrid modes are presented. The mode matching at the entrance of the CC-waveguide is described. The components of electromagnetic fields of obliquely incident gaussian beam at the entrance of the CC-waveguide are calculated. In section 3, the numerical calculation of coupling in the ECH transmission system of the large helical device (LHD) is carried out. The values of off-axis shift and tilting angle are discussed to satisfy the specific coupling efficiency. For a general application, coupling

dependence on waveguide size and frequency for an obliquely or off-axis incident beam is shown and its characteristics are described. By changing the gaussian beam for the HE_{11} mode, effects of the tilting and offset of the CC-waveguide on coupling efficiency are given. Conclusion is given in section 4.

2 Theoretical consideration

2.1 Electromagnetic fields

In the cartesian coordinate system where the origin of (x, y, z) is located at the center of the CC-waveguide aperture, EM fields of TEM_{nm} mode with the waist point $z_0 = 0$ are given by [8]

$$\begin{aligned} E_y &= \frac{\epsilon_n}{w}\sqrt{\frac{2Z_0 m!}{\pi(m+n)!}}\left(\frac{\sqrt{2}\,r}{w}\right)^n L_m^n\left(\frac{2r^2}{w^2}\right)\exp\left[-r^2\left(\frac{1}{w^2}+\frac{jk}{2R}\right)\right] \\ &\quad \times \cos n\phi\,\exp\left[-jkz + j(2m+n+1)\tan^{-1}\left(\frac{\lambda z}{\pi w_0^2}\right)\right], \end{aligned} \tag{1}$$

$$H_x = -E_y/Z_0, \tag{2}$$

where, $Z_0 = \sqrt{\mu_0/\epsilon_0}$, $R = z(1 + (\pi w_0^2/\lambda z)^2)$, $w = w_0\sqrt{1 + (\lambda z/\pi w_0^2)^2}$ and $\phi = \tan^{-1}(y/x)$ and L_m^n is the generalized Laguerre's polynomial and w_0 is waist size at the waist point, and ϵ_n= 1 or $1/\sqrt{2}$ for $n = 0$ and 1, respectively.

For the hybrid mode with the mode number of (n, m) in the azimuthal and axial directions and the eigen value X_m, EM fields [9] can be written by

$$\begin{pmatrix} E_x \\ E_y \\ E_z \end{pmatrix} = G_m \begin{pmatrix} \sin(n-1)\phi & -\sin(n+1)\phi & 0 \\ \cos(n-1)\phi & \cos(n+1)\phi & 0 \\ 0 & 0 & \sin n\phi \end{pmatrix}$$

$$\times \begin{pmatrix} (1-d_m)J_{n-1}\left(\frac{X_m r}{a}\right) \\ (1+d_m)J_{n+1}\left(\frac{X_m r}{a}\right) \\ \frac{j2X_m}{R_m Y}J_n\left(\frac{X_m r}{a}\right) \end{pmatrix} \exp(-j\beta_m z), \tag{3}$$

$$\begin{pmatrix} H_x \\ H_y \\ H_z \end{pmatrix} = F_m \begin{pmatrix} -\cos(n-1)\phi & -\cos(n+1)\phi & 0 \\ \sin(n-1)\phi & -\sin(n+1)\phi & 0 \\ 0 & 0 & \cos n\phi \end{pmatrix}$$

$$\times \begin{pmatrix} (1-d_m R_m^2) J_{n-1}(\frac{X_m r}{a}) \\ (1+d_m R_m^2) J_{n+1}(\frac{X_m r}{a}) \\ \frac{j2X_m d_m R_m}{Y} J_n(\frac{X_m r}{a}) \end{pmatrix} \exp(-j\beta_m z). \tag{4}$$

The cross-polarized field is obtained by substituting the cosine function for the sine one and the $-$sine function for the cosine one. Here, d_m, R_m, G_m and F_m are defined as

$$d_m = \begin{cases} \dfrac{J_{n-1}(X_m)+J_{n+1}(X_m)}{J_{n-1}(X_m)-J_{n+1}(X_m)}, & n \neq 0 \\ 1, & \text{for} \quad \mathrm{TE_{0m}} \\ -\dfrac{J_0(X_m)}{X_m J_1(X_m)}, & \text{for} \quad \mathrm{TM_{0m}}, \end{cases} \tag{5}$$

$$R_m = \beta_m/k = \sqrt{[1-(X_m/Y)^2]}; \qquad Y = ka, \tag{6}$$

$$G_m = \frac{\sqrt{R_m Z_0}}{2a\sqrt{\pi D_m} J_n(X_m)}, \tag{7}$$

$$F_m = \frac{1}{2a\sqrt{\pi D_m R_m Z_0} J_n(X_m)}, \tag{8}$$

where $k = \omega/c = 2\pi/\lambda$ and

$$D_m = \begin{cases} \dfrac{1}{2}\Big[\Big(1-\dfrac{n^2}{X_m^2}+\dfrac{2n}{d_m X_m^2}+\dfrac{n^2}{d_m^2 X_m^2}\Big) \\ \times(1+R_m^2 d_m^2) - 2(1+R_m^2)\dfrac{n d_m}{X_m^2}\Big], & n \neq 0 \\ 1-\dfrac{2}{YZ}+\Big(\dfrac{X_m}{YZ}\Big)^2, & \text{for} \quad \mathrm{TM_{0m}} \\ R_m^2, & \text{for} \quad \mathrm{TE_{0m}}. \end{cases} \tag{9}$$

Here, the normalized reactance Z along z-direction [9] is given by

$$Z = \frac{j}{Z_0}\Big[\frac{E_z}{H_\phi}\Big]_{r=a} = \begin{cases} \dfrac{X_m^2 d_m}{nY(d_m^2 R_m^2 - 1)}, & n \neq 0 \\ -\dfrac{X_m^2 d_m}{Y}, & \text{for} \quad \mathrm{TM_{0m}}. \end{cases} \tag{10}$$

For the $\mathrm{TM_{0m}}$ mode, equations describing the cross-polarized field should be used to calculate electromagnetic field. To calculate EM-field, it is necessary that X_m is determined. By using the Newton-Raphson method to solve the equation, X_m can be represented as a function of d. For the sake of simplicity, we use the ideal eigenvalue X_m satisfying $J_{n-1}(X_m) = 0$ for HE_{nm}, $J_{n+1}(X_m) = 0$ for $\mathrm{EH}_{n,m+1}$ and $J_0'(X_m) = -J_1(X_m) = 0$ for TM_{0m}, since both Z and $2a$ have large values in this analysis. All the numerical coefficients of EM fields in gaussian beam and hybrid mode are normalized so as to satisfy flux $P = \iint_S (\boldsymbol{E} \times \boldsymbol{H}^*) \cdot d\boldsymbol{S} = 1$ where $\boldsymbol{S}$ is the whole plane of a cross section.

2.2 Evaluation of coupling coefficients

In the waveguide system, the following orthonormal relation between the i- and j-modes is valid:

$$\iint_S (\boldsymbol{E}_i \times \boldsymbol{H}_j^*) \cdot d\boldsymbol{S} = \delta_{ij}, \tag{11}$$

where S is the cross-section of the CC-waveguide and δ_{ij} is 1 for $i = j$ and 0 for $i \neq j$. The injected gaussian beam $\boldsymbol{E}(x, y, 0)$ and $\boldsymbol{H}(x, y, 0)$ at the plane of the waveguide aperture is expanded as

$$\boldsymbol{E} = \Sigma A_j \boldsymbol{E}_j + \boldsymbol{E}_{out}, \tag{12}$$

$$\boldsymbol{H} = \Sigma A_j \boldsymbol{H}_j + \boldsymbol{H}_{out}, \tag{13}$$

where A_j is the amplitude of the EM field for the j-mode, and $\boldsymbol{E}_{out}(\boldsymbol{H}_{out})$ is the EM field outside the waveguide. Because the orthonormality in the waveguide is satisfied, the coefficient A_j is calculated from

$$A_j = \iint_S (\boldsymbol{E} \times \boldsymbol{H}_j^*) \cdot d\boldsymbol{S} = \iint_S (\boldsymbol{E}_j \times \boldsymbol{H}^*)^* \cdot d\boldsymbol{S}. \tag{14}$$

The power content of j-mode in the waveguide is equal to $|A_j|^2$. For the $\mathrm{TEM_{00}}$ mode, the calculation of A_j is straightforward

$$A_j = -\iint_S E_{jy}^* H_x \, dx \, dy. \tag{15}$$

At the same time, the normalized flux of $\mathrm{TEM_{00}}$ mode to waveguide is calculated by

$$P_{\mathrm{WG}} = \frac{1}{Z_0} \iint_S |\, E_y \,|^2 \cos\alpha \cos\beta \, dx \, dy. \tag{16}$$

Here, if the center of waist point is located at $z_0'(\neq 0)$, z' variable should be substituted by $z' - z_0'$. To calculate A_j, the two dimensional data sampled with $M \times M$ on the plane $(x, y, 0)$ are provided for both injected gaussian beam and waveguide mode. For the numerical calculation in the following section, we use 64×64 sampling points and the radius of 16 sampling points for the CC-waveguide. In order to examine the coupling efficiencies in the ECH system for the LHD, the numerical integration in two dimensions is carried out for waveguide modes of HE_{nm}, EH_{nm}, TE_{0m} and TM_{0m}.

2.3 Oblique incidence of gaussian beam

As shown in Fig. 1, for an on-axis gaussian beam injected with a small angle, injected EM fields at the entrance of waveguide are calculated. The cartesian coordinate

system (x', y', z') rotated by α and β around x- and y-axes of the (x, y, z) coordinate system is transformed as:

$$\begin{pmatrix} x' \\ y' \\ z' \end{pmatrix} = \begin{pmatrix} \cos\beta & 0 & 0 \\ \sin\alpha\sin\beta & \cos\alpha & 0 \\ \cos\alpha\sin\beta & \sin\alpha & 0 \end{pmatrix} \begin{pmatrix} x \\ y \\ z \end{pmatrix}. \tag{17}$$

When we consider the gaussian beam of TEM_{00} with E'_y and H'_x, magnetic field H_x is given by

$$H_x = H'_x(x', y', z')\cos\beta. \tag{18}$$

3 Numerical calculation

In the LHD, the transmission lines which consists of the CC-waveguide with $2a$ = 88.9mm for $\omega/2\pi$=84 and 168 GHz are being prepared. In this section, the result from the coupling calculation based on those parameters is discussed. When the gaussian beam with waist point z_0 located at the entrance of the CC-waveguide is injected normally, the contours of P_{WG} and $|A_{\mathrm{HE11}}|^2$ in the (z_0, w_0) plane for $\omega/2\pi$=168 GHz are shown in Figs.2 (a)-(b).

The flux P_{WG} has small dependence on z_0 in the range of $|\, z_0 \,| \leq 500$ mm. It is found from Fig. 2 (b) that the maximum of $|A_{\mathrm{HE11}}|^2$ is in w_0/a=0.643 and z_0=0, and that those values agree well with the theoretical analysis by [6], [7]. It becomes evident that for large w_0, most of P_{WG} is coupled to HE_{11} mode and that for small w_0, mode purity in the waveguide decreases. As shown in Fig. 2 (c), z_0 and w_0 at which the coupling is maximum of $|A_{\mathrm{HE11}}|^2$ for $\omega/2\pi$=84 GHz are the same as that in Fig. 2 (b). In comparison with the result from $\omega/2\pi$=168 GHz, the dependence of $|A_{\mathrm{HE11}}|^2$ on z_0 increases due to the smaller R of wavefront at the entrance. As a result, the maximum coupling for larger z_0 increases slightly from w_0/a=0.643.

In Fig. 3 (a), contours of $|A_{\mathrm{HE11}}|^2$ are plotted in the (w_0, α) plane for $\omega/2\pi$=168 GHz and $2a$=88.9 mm. Here, the angle α is equal to the deviation from the normal incidence. With increasing α, the optimum w_0 decreases from w_0/a=0.643. It is noted that $|A_{\mathrm{HE11}}|^2$ for α = 1deg is as small as 0.45, even if $P_{\mathrm{WG}} \geq 0.98$. For the gaussian beam with the smaller w_0, dependence of $|A_{\mathrm{HE12}}|^2$ on α is weak since the main body of gaussian beam is located only near the axis and then the effect to the coupling due to the phase variation is weakened on an average. For reference, $|A_{\mathrm{XHE21}}|^2$, $|A_{\mathrm{TM02}}|^2$ and $|A_{\mathrm{HE12}}|^2$ are plotted in the (w_0, α) plane in Figs. 3 (b) and (c). For tilting, the HE_{12} mode is almost independent of α; however, XHE_{21} and TM_{02} modes are created as a result of non-uniformity of phase on the entrance.

In Figs. 4 (a)-(b), contours of $|A_{\mathrm{HE11}}|^2$, $|A_{\mathrm{HE21}}|^2$ and $|A_{\mathrm{TE01}}|^2$ are plotted in the (w_0, y_d) plane for the normal incidence. Here, y_d is the displacement value of gaussian beam along the y-axis. The optimum value of w_0 increases with offset. Even for y_d equal to 5 mm, $|A_{\mathrm{HE11}}|^2$ is more than 0.9 because the phase distribution remains constant and only the amplitude becomes asymmetric. In Figs. 5 (a)-(c), contours of P_{WG}, $|A_{\mathrm{HE11}}|^2$, $|A_{\mathrm{HE21}}|^2$ and $|A_{\mathrm{TE01}}|^2$, $|A_{\mathrm{XHE21}}|^2$ and $|A_{\mathrm{TM02}}|^2$ are plotted in the (x_d, y_d) plane for normal incidence, where x_d is the offset value of gaussian beam along the x-axis. It is noted that the contours of P_{WG} and $|A_{\mathrm{HE11}}|^2$ show axisymmetry. For $r_d/a = \sqrt{x_d^2 + y_d^2}/a \leq 0.02$, $|A_{\mathrm{HE11}}|^2$ is nearly equal to 0.9 even if $P_{\mathrm{WG}} \simeq 0.98$. The off-axis shift should be less than 2.9 mm for mode-conversion loss of $\leq$1 %. The polynomial fitting of Fig. 5 (b) is

$$|A_{\mathrm{HE11}}|^2 \simeq 0.98 - 1.2 \times 10^{-3} r_d^2 + 5.6 \times 10^{-7} r_d^4, \tag{19}$$

for $r_d \leq$20 mm. The normalized mode conversion loss can be written as

$$|A_{\mathrm{HE11}}|^2 \simeq 0.98 - 2.3(r_d/a)^2 + 2.2(r_d/a)^4, \tag{20}$$

for $r_d/a \leq 0.45$ In Figs. 6 (a)-(c), the contours of $|A_{\mathrm{HE11}}|^2$, $|A_{\mathrm{HE21}}|^2$ and $|A_{\mathrm{TE01}}|^2$, $|A_{\mathrm{XHE21}}|^2$ and $|A_{\mathrm{TM02}}|^2$ are plotted in the (α, β) plane with $x_d = y_d = 0$. Contours of $|A_{\mathrm{HE11}}|^2$ $|A_{\mathrm{HE12}}|^2$, are axisymmetric. It is confirmed that power conservation $P_{\mathrm{WG}} \simeq \sum |A_{\mathrm{MODE}}|^2$ is valid within n=3 and m=3. At $\alpha \simeq 0.5$ and $\beta = 0$, higher modes of 14% which mainly consist of $|A_{\mathrm{XHE21}}|^2$ and $|A_{\mathrm{TM02}}|^2$ are excited, however, a small content of the HE_{12} mode with axisymmetric contour exists as well. In Figs. 7 (a)-(b), P_{WG} and $\sum |A_{\mathrm{MODE}}|^2$ are plotted as a function of α and β, respectively. In α (or β) $\simeq$ 0.16 deg where $|A_{\mathrm{HE11}}|^2$ decreases to 0.96, $|A_{\mathrm{HE12}}|^2$ is equal to $|A_{\mathrm{XHE21}}|^2$ and $|A_{\mathrm{TM02}}|^2$ ($|A_{\mathrm{HE21}}|^2$ and $|A_{\mathrm{TE01}}|^2$). For $\omega/2\pi$=84 GHz, the same figures as Figs. 7 (a) and (b) are obtained by exchanging the scale (-1 to 1) of α and β-axes to scale (-2 to 2). To suppress the total higher mode content to a value less than 1%, the tilting angle should be less than 0.1 deg for $\omega/2\pi$=168 GHz and $2a$=88.9 mm. By comparing Fig. 7 (a) with Fig. 7 (b), the curves in (b) are easily obtained by exchanging the label of modes to the cross polarization mode.

As shown in Fig. 8, the contours $|A_{\mathrm{HE11}}|^2$ for w_0/a=0.643 are plotted in the $(1/2a, \alpha)$ plane as a parameter of $|A_{\mathrm{HE11}}|^2$. All the contour curves are straight lines passing through the origin (0, 0) if each line is extrapolated. In the approximation of $\tan\alpha \simeq \alpha$, α is inversely proportional to a for constant $|A_{\mathrm{HE11}}|^2$. Taking into account axisymmetry of $|A_{\mathrm{HE11}}|^2$, it is found that $|A_{\mathrm{HE11}}|^2$ depends on the product of $a\theta$, where $\theta = \sqrt{(\alpha^2 + \beta^2)}$. The result shows that the careful adjustment of incident angle is required for effectual transmission in the large diameter of the CC-waveguide.

In Fig. 9 (a), contours of $|A_{\mathrm{HE11}}|^2$ are plotted in the $(\lambda, 2a)$ plane for the fixed angle of α=0.1 deg and w_0/a=0.643. In Fig. 9 (b), contours are also plotted as a parameter of the incident angle when $|A_{\mathrm{HE11}}|^2$=0.970 and w_0/a=0.643. In both graphs, all the lines pass through the origin (0, 0). For the ECH experimental ranges of $2a$=50 $\sim$100 mm and 60$\sim$200 GHz in the device such as LHD, Wendelstein-7 AS [4], Heliotron-E [3], and ITER [10] if the injection angle can be adjusted so as to satisfy $|\alpha| \leq$0.1 deg, the power coupling efficiency more than 97% is achieved. From both figures, it is found that $|A_{\mathrm{HE11}}|^2$ depends on a/λ. By considering the discussion in Fig. 8, it becomes evident that $|A_{\mathrm{HE11}}|^2$ is a function of $a\theta/\lambda$. In order to obtain the scaling formula, polynomial fitting of $|A_{\mathrm{HE11}}|^2$ in Fig. 6 is carried out in the range of $|\alpha| \leq 1$ deg:

$$|A_{\mathrm{HE11}}|^2 \simeq 0.98 - 0.73\alpha^2 + 0.20\alpha^4, \tag{21}$$

where the unit of α is degree. By introducing the dependence of $a\theta/\lambda$ on coupling coefficient for general injection angle θ , the above equation is rewritten as

$$|A_{\mathrm{HE11}}|^2 \simeq 0.98 - 3.9(a\theta/\lambda)^2 + 5.6(a\theta/\lambda)^4, \tag{22}$$

for $|a\theta/\lambda| \leq$0.43, where the unit of θ is radian. When the tilting gaussian beam is injected with offset, the total mode conversion loss is approximately given by sum of the loss terms of Eqs. (20) and (22)).

To confirm formulas of the mode-conversion loss at the junction of the CC-waveguide with tilt or offset [5], the EM fields of HE_{11} mode instead of the gaussian beam are used. The mode conversion loss at the junction of CC-waveguides obtained is written as

$$|A_{\mathrm{HE11}}|^2 \simeq 1 - 2.7(r_d/a)^2 + 3.2(r_d/a)^4, \tag{23}$$

for offset of the waveguide axis ($r_d/a \leq .45$) and

$$|A_{\mathrm{HE11}}|^2 \simeq 1 - 4.2(a\theta/\lambda)^2 + 6.3(a\theta/\lambda)^4, \tag{24}$$

for tilting of the axis ($|a\theta/\lambda| \leq$0.43). The mode-conversion loss by the small offset and tilting are close to the results (Eqs. (20) and (22)) from gaussian beam injection and the calculations by coupled mode theory reported previously [5].

In analysis of the oversized miter bend, the input EM-field to the phase-corrected reflecting mirror in the bend is treated as the radiated fields from the CC-waveguide [11, 12]. The mode-conversion loss for a 90-degree plane miter bend is given by $0.74(\lambda/a)^{3/2}$. For instance, in the 90-degree miter bend, the setting accuracies on the angle and position of the reflecting mirror are closely related with the oblique and off-axis injection of gaussian beam, even though the near-field radiation from the CC-waveguide is not able to approximate as the only fundamental gaussian beam [13]. The setting tolerance on the angle and position of reflecting mirror is inferred to be similar to results from the present analysis.

4 Conclusion

The mode-conversion loss increases and the optimum w_0 changes when the gaussian beam is injected with offset or tilt into the circular corrugated waveguide. For the gaussian beam with waist size of w_0/a=0.643, the power losses depend on $2.3(r_d/a)^2 - 2.2(r_d/a)^4$ and $3.9(a\theta/\lambda)^2 - 5.6(a\theta/\lambda)^4$ for offset and tilt, respectively. In the recent high power ECH system, large diameter of waveguide and high frequency more than 100 GHz are required from the viewpoint of breakdown and penetration of millimeter waves to the core in the high density plasmas. It is pointed out that the careful alignment of injection beam to the CC-waveguide is necessary for such requirement and that deviation angle of injection from the axis and offset should be less than 0.1 degrees and 2.9 mm to achieve the loss of $\leq 1\%$ for LHD.

Acknowledgments

The authors would like to thank Drs. T. Watari, M. Fujiwara and A. Iiyoshi for their continuing encouragements. They also acknowledge Dr. M. Pereyaslavets for his discussion and Dr. H. Nagasaki for the application of this analysis to the ECH transmission system in Heliotron-E.

References

[1] Ohkubo, K., Kubo, S., Iwase, M., Idei, H., Sato, M., Shimozuma, T., Takita, Y. and Kuroda, T., *International Journal of Infrared and Millimeter Waves*, **15**, 1507-1519, 1994.

[2] Moeller, C., Prater, R., Callis, R., Remsen, D., Doanne, J., Cary, W., Phelps, R. and Tupper, M., *Proceedings of the 16th Symposium on Fusion Technology*, vol. 2, 1040-1044 (Elsevier, Amsterdam), 1991.

[3] Nagasaki, H., Zushi, H., Sato, M., Sano, F., Kondo, K., Sudo, S., Mizuuchi, T., Besshou, S., Okada, H., Iima, M., Kobayashi, S., Isayama, A. and Obiki, T., *Fusion Technology*, **26**, 153-158, 1995.

[4] Erckmann, V., Gantenbein, G., Garaubner, T., Kasparek, W., Kunrić, H., Müller, G.A., Schüller, P.G. and Wagner, G., *Proceedings of the 19th International Conference on Infrared and Millimeter Waves*, Sendai, 236-237, 1994.

[5] Thumm, M. and Kasparek, W., *Fusion Engineering and Design*, **26**, 291-317, 1995.

[6] Abrams, P.L. *IEEE Journal of Quantum. Electronics*, **QE – 8**, 838-818, 1972.

[7] Roullard, E.P. and Bass, M., *IEEE Journal of Quantum Electronics*, **Q13**, 813-818, 1972.

[8] Yariv, A., *Quantum Electronics*, (Wiley, New York), 1975.

[9] Doanne, J. *Infrared and Millimeter Waves*, Chapter 5, Propagation and mode coupling in corrugated and smooth-wall circular waveguides, p123-170 (Academic Press, New York), 1985.

[10] Makowski, M., Private Communication in *International Workshop on ECH Transmission System*, Cocoa Beach Florida, 1995.

[11] Vaganov, R.B., *Radio Engineering and Electronic Physics*, **18**, 170-175, 1973.

[12] Ohkubo, K., Kubo S., Iwase, M., Idei, H. Sato, M., Shimozuma, T., Takita, Y., and Kuroda, T., *Proceedings of the 18th Symposium on Fusion Technology*, vol. 1, 513-516 (Elsevier, Amsterdam), 1995.

[13] Rebuffi, S. and Crenn, J.P., *International Journal of Infrared and Millimeter Waves*, **10**, 291-311, 1989.

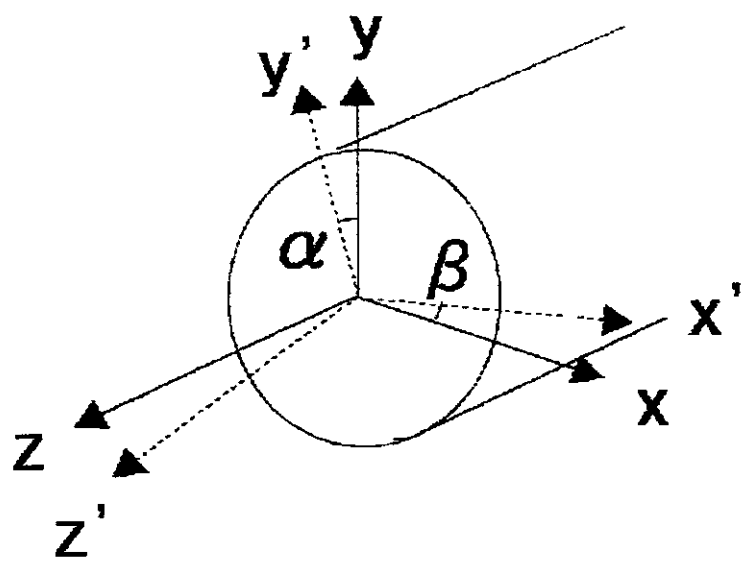

Fig. 1: Schematic drawing of the gaussian beam injected into the entrance of the waveguide. Here, the angle α and β correspond to the rotation around the x- and y-axis, respectively.

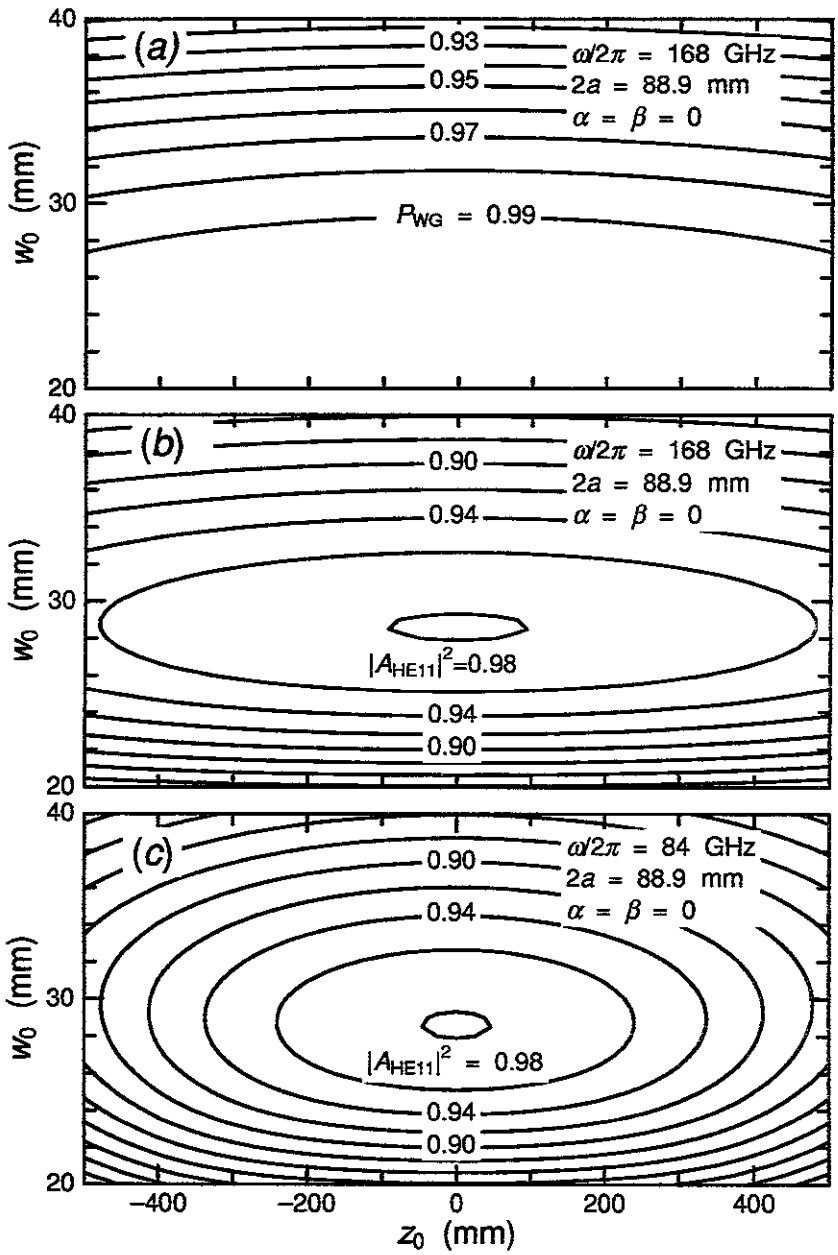

Fig. 2: Contour plots of (a) P_{WG}, (b) $|A_{\mathrm{HE11}}|^2$ for $\omega/2\pi$=168 GHz, and (c) $|A_{\mathrm{HE11}}|^2$ for $\omega/2\pi$=84 GHz for normally injected beam at the entrance of the waveguide with $2a$=88.9 mm.

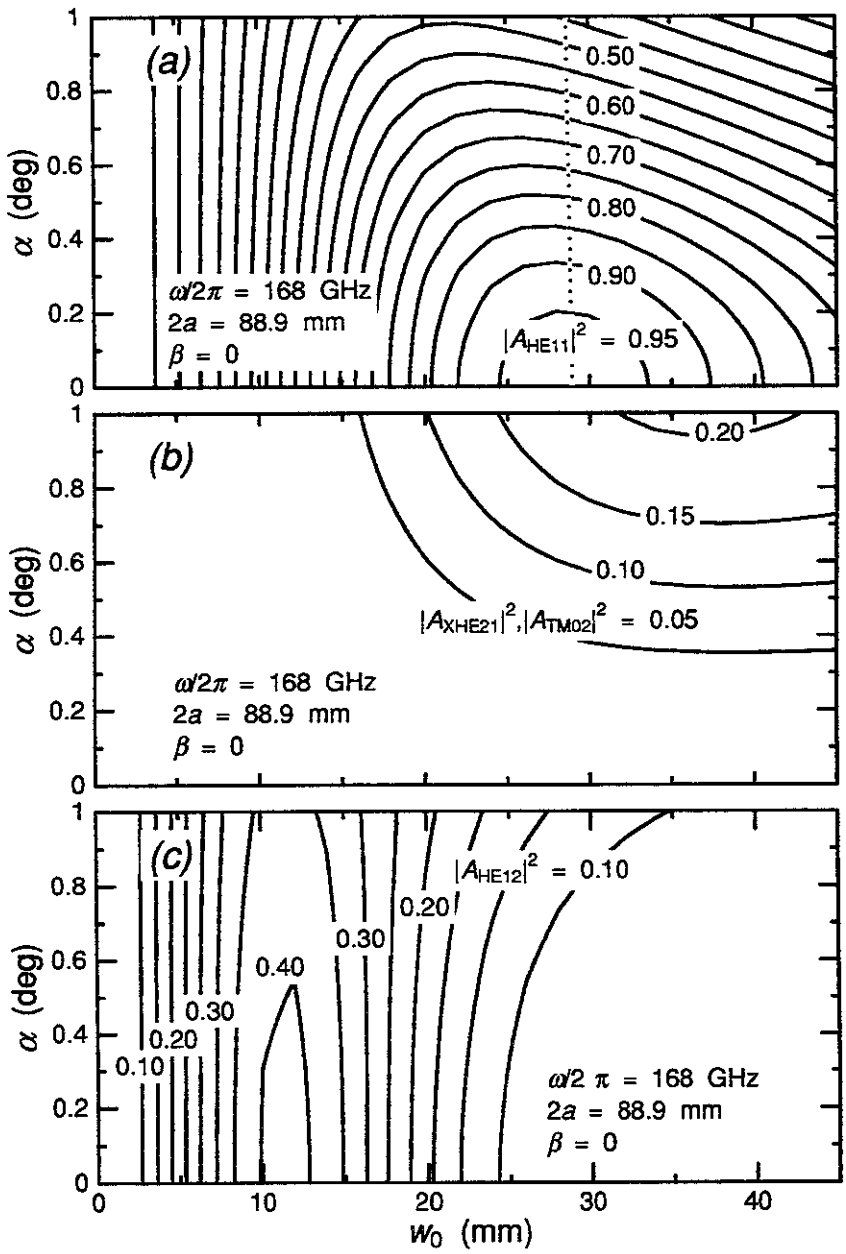

Fig. 3: Contour plots of (a) $|A_{\mathrm{HE11}}|^2$, (b) $|A_{\mathrm{XHE21}}|^2$ and $|A_{\mathrm{TM02}}|^2$, (c) $|A_{\mathrm{HE12}}|^2$ in the (w_0, α) plane for $\omega/2\pi$=168 GHz, and $2a$=88.9 mm when a gaussian beam TEM_{00} is injected with x_d=y_d=0.

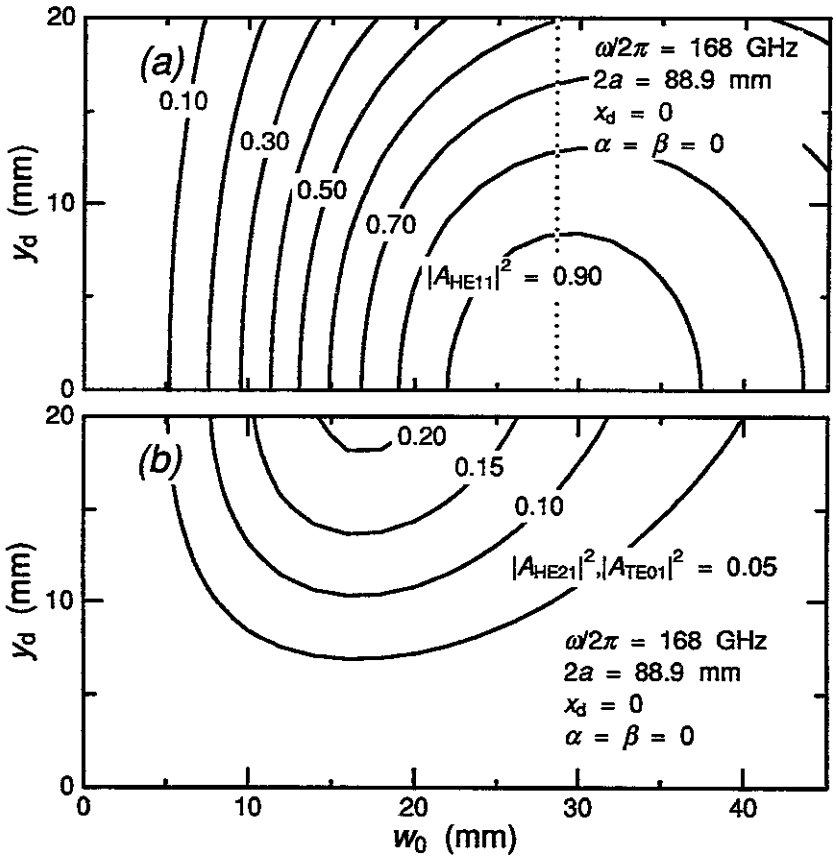

Fig. 4: Contour plots of (a) $|A_{\mathrm{HE11}}|^2$, (b) $|A_{\mathrm{HE21}}|^2$ and $|A_{\mathrm{TE01}}|^2$, in the (w_0, y_d) plane for $\omega/2\pi$=168 GHz, and $2a$=88.9 mm when a gaussian beam TEM_{00} is injected with x_d=0 and α=β=0.

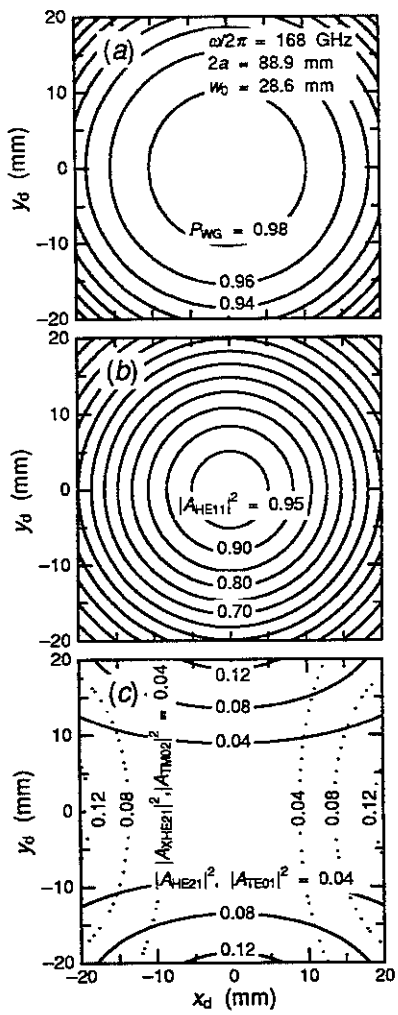

Fig. 5: Contour plots of (a) P_{WG}, (b) $|A_{\mathrm{HE11}}|^2$, (c) $|A_{\mathrm{HE21}}|^2$ and $|A_{\mathrm{TE01}}|^2$, $|A_{\mathrm{XHE21}}|^2$ and $|A_{\mathrm{TM02}}|^2$ in the (x_d, y_d) plane for $\omega/2\pi =$ 168 GHz when a gaussian beam $\mathrm{TEM_{00}}$ with $w_0/a = 0.643$ is injected normally to the entrance of the waveguide with $2a = 88.9$ mm.

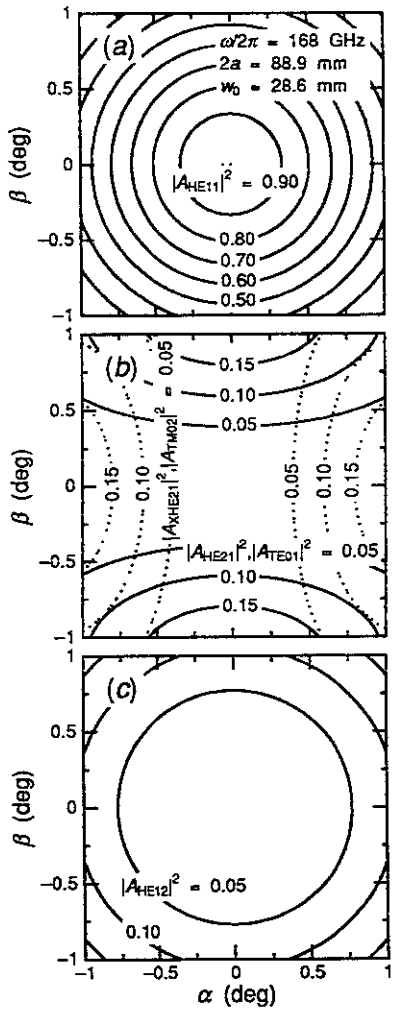

Fig. 6: Contour plots of (a) $|A_{\mathrm{HE11}}|^2$, (b) $|A_{\mathrm{HE21}}|^2$ and $|A_{\mathrm{TE01}}|^2$, $|A_{\mathrm{XHE21}}|^2$ and $|A_{\mathrm{TM02}}|^2$, (c) $|A_{\mathrm{HE12}}|^2$ in the (α, β) plane for $\omega/2\pi = 168$ GHz when a gaussian beam $\mathrm{TEM_{00}}$ with $w_0/a = 0.643$ is injected obliquely into the center ($x_d = y_d = 0$) of the CC-waveguide with $2a$=88.9 mm.

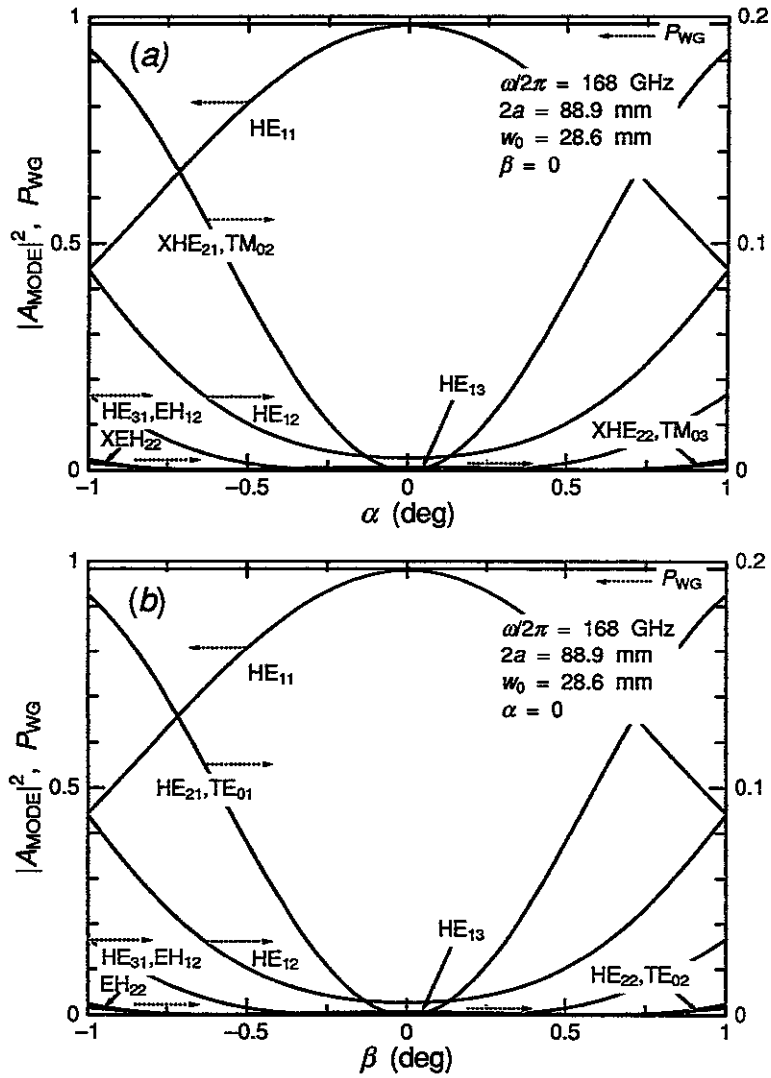

Fig. 7: (a) P_{WG} and $|A_{\mathrm{MODE}}|^2$ are plotted as a function of α. Here, MODE denotes HE_{11}, XHE_{21} and TM_{02}, HE_{12}, HE_{31} and EH_{12}, XEH_{22}, XHE_{22} and TM_{03}, HE_{13}, respectively. (b) P_{WG} and $|A_{\mathrm{MODE}}|^2$ are plotted as a function of β. Here, MODE denotes HE_{11}, HE_{21} and TE_{01}, HE_{12}, HE_{31} and EH_{12}, EH_{22}, HE_{22} and TE_{02}, HE_{13}, respectively.

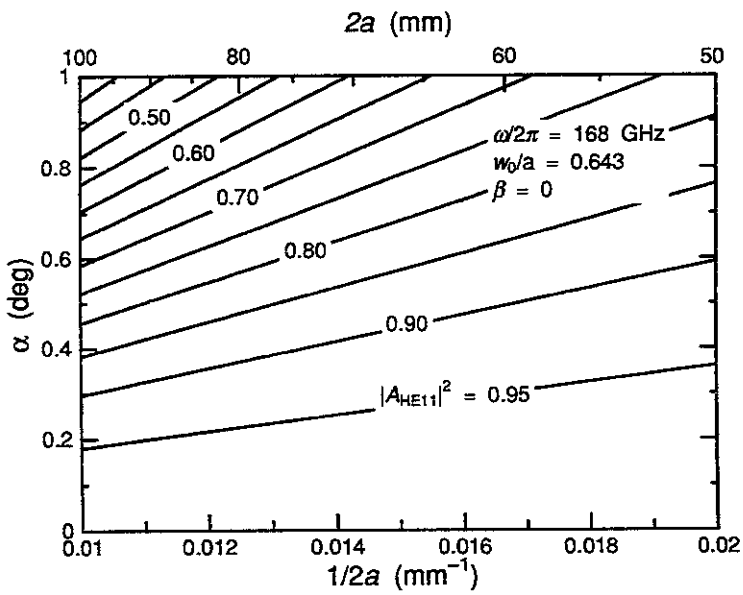

Fig. 8: Contour plots of $|A_{\mathrm{HE11}}|^2$ in the $(1/2a, \alpha)$ plane for $\omega/2\pi$=168 GHz and β=0 when a gaussian beam TEM_{00} with w_0/a=0.643 is injected obliquely into the center of the CC-waveguide. All the lines pass through the origin (0, 0).

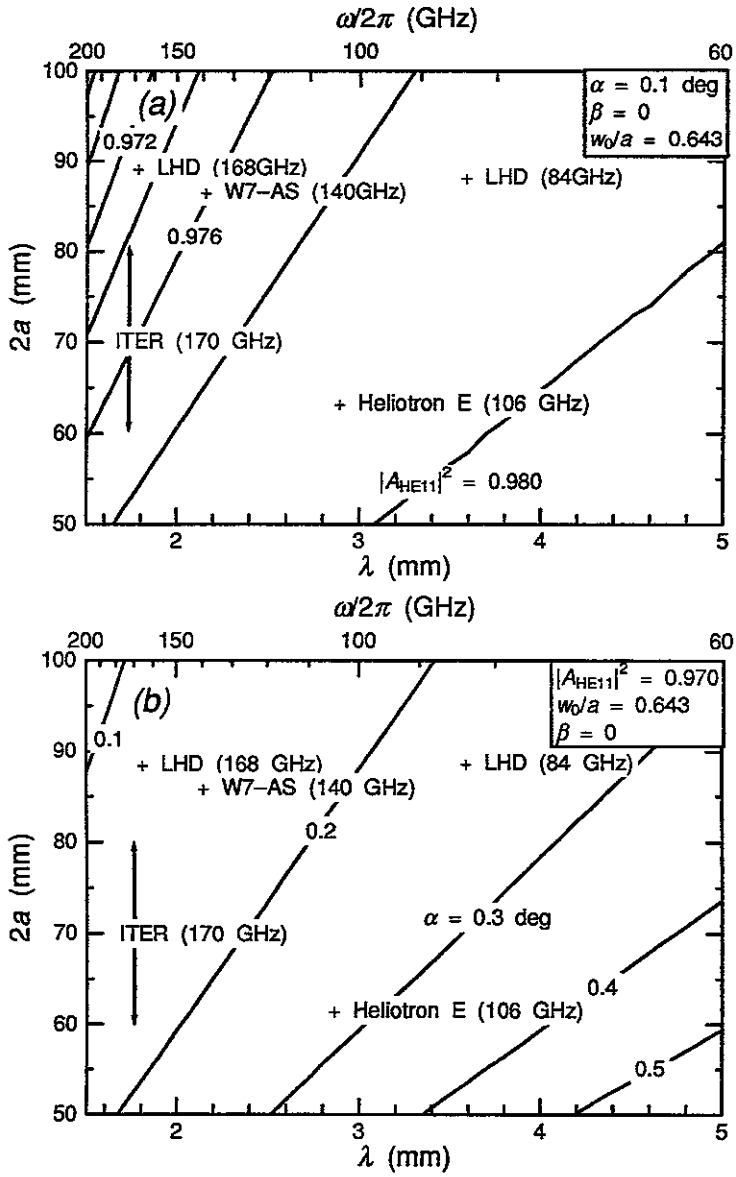

Fig. 9: (a) Contour plots of $|A_{\mathrm{HE11}}|^2$ in the $(\lambda, 2a)$ plane for α=0.1 deg and β=0 when a gaussian beam $\mathrm{TEM_{00}}$ with w_0/a=0.643 is injected. All the lines pass through the origin (0, 0). (b) Contour plots of α in the $(\lambda, 2a)$ plane for satisfying $|A_{\mathrm{HE11}}|^2$=0.970 when a gaussian beam $\mathrm{TEM_{00}}$ with w_0/a=0.643 is injected with β=0. All the lines pass through the origin (0, 0).

Recent Issues of NIFS Series

NIFS-435 H. Sugama and W. Horton.
Transport Processes and Entropy Production in Toroidally Rotating Plasmas with Electrostatic Turbulence; Aug. 1996

NIFS-436 T. Kato, E. Rachlew-Källne, P. Hörling and K.-D Zastrow,
Observations and Modelling of Line Intensity Ratios of OV Multiplet Lines for 2s3s 3S1 - 2s3p 3Pj; Aug. 1996

NIFS-437 T. Morisaki, A. Komori, R. Akiyama, H. Idei, H. Iguchi, N. Inoue, Y. Kawai, S. Kubo, S. Masuzaki, K. Matsuoka, T. Minami, S. Morita, N. Noda, N. Ohyabu, S. Okamura, M. Osakabe, H. Suzuki, K. Tanaka, C. Takahashi, H. Yamada, I. Yamada and O. Motojima,
Experimental Study of Edge Plasma Structure in Various Discharges on Compact Helical System; Aug. 1996

NIFS-438 A. Komori, N. Ohyabu, S. Masuzaki, T. Morisaki, H. Suzuki, C. Takahashi, S. Sakakibara, K. Watanabe, T. Watanabe, T. Minami, S. Morita, K. Tanaka, S. Ohdachi, S. Kubo, N. Inoue, H. Yamada, K. Nishimura, S. Okamura, K. Matsuoka, O. Motojima, M. Fujiwara, A. Iiyoshi, C. C. Klepper, J.F. Lyon, A.C. England, D.E. Greenwood, D.K. Lee, D.R. Overbey, J.A. Rome, D.E. Schechter and C.T. Wilson,
Edge Plasma Control by a Local Island Divertor in the Compact Helical System; Sep. 1996 (IAEA-CN-64/C1-2)

NIFS-439 K. Ida, K. Kondo, K. Nagaski T. Hamada, H. Zushi, S. Hidekuma, F. Sano, T. Mizuuchi, H. Okada, S. Besshou, H. Funaba, Y. Kurimoto, K. Watanabe and T. Obiki,
Dynamics of Ion Temperature in Heliotron-E; Sep. 1996 (IAEA-CN-64/CP-5)

NIFS-440 S. Morita, H. Idei, H. Iguchi, S. Kubo, K. Matsuoka, T. Minami, S. Okamura, T. Ozaki, K. Tanaka, K. Toi, R. Akiyama, A. Ejiri, A. Fujisawa, M. Fujiwara, M. Goto, K. Ida, N. Inoue, A. Komori, R. Kumazawa, S. Masuzaki, T. Morisaki, S. Muto, K. Narihara, K. Nishimura, I. Nomura, S. Ohdachi, M.. Osakabe, A. Sagara, Y. Shirai, H. Suzuki, C. Takahashi, K. Tsumori, T. Watari, H. Yamada and I. Yamada,
A Study on Density Profile and Density Limit of NBI Plasmas in CHS; Sep. 1996 (IAEA-CN-64/CP-3)

NIFS-441 O. Kaneko, Y. Takeiri, K. Tsumori, Y. Oka, M. Osakabe, R. Akiyama, T. Kawamoto, E. Asano and T. Kuroda,
Development of Negative-Ion-Based Neutral Beam Injector for the Large Helical Device; Sep. 1996 (IAEA-CN-64/GP-9)

NIFS-442 K. Toi, K.N. Sato, Y. Hamada, S. Ohdachi, H. Sakakita, A. Nishizawa, A. Ejiri, K. Narihara, H. Kuramoto, Y. Kawasumi, S. Kubo, T. Seki, K. Kitachi, J. Xu, K. Ida, K. Kawahata, I. Nomura, K. Adachi, R. Akiyama, A. Fujisawa, J. Fujita, N. Hiraki, S. Hidekuma, S. Hirokura, H. Idei, T. Ido, H. Iguchi, K. Iwasaki, M.

Isobe, O. Kaneko, Y. Kano, M. Kojima, J. Koog, R. Kumazawa, T. Kuroda, J. Li, R. Liang, T. Minami, S. Morita, K. Ohkubo, Y. Oka, S. Okajima, M. Osakabe, Y. Sakawa, M. Sasao, K. Sato, T. Shimpo, T. Shoji, H. Sugai, T. Watari, I. Yamada and K. Yamauti,
Studies of Perturbative Plasma Transport, Ice Pellet Ablation and Sawtooth Phenomena in the JIPP T-IIU Tokamak; Sep. 1996 (IAEA-CN-64/A6-5)

NIFS-443 Y. Todo, T. Sato and The Complexity Simulation Group,
Vlasov-MHD and Particle-MHD Simulations of the Toroidal Alfvén Eigenmode; Sep. 1996 (IAEA-CN-64/D2-3)

NIFS-444 A. Fujisawa, S. Kubo, H. Iguchi, H. Idei, T. Minami, H. Sanuki, K. Itoh, S. Okamura, K. Matsuoka, K. Tanaka, S. Lee, M. Kojima, T.P. Crowley, Y. Hamada, M. Iwase, H. Nagasaki, H. Suzuki, N. Inoue, R. Akiyama, M. Osakabe, S. Morita, C. Takahashi, S. Muto, A. Ejiri, K. Ida, S. Nishimura, K. Narihara, I. Yamada, K. Toi, S. Ohdachi, T. Ozaki, A. Komori, K. Nishimura, S. Hidekuma, K. Ohkubo, D.A. Rasmussen, J.B. Wilgen, M. Murakami, T. Watari and M. Fujiwara,
An Experimental Study of Plasma Confinement and Heating Efficiency through the Potential Profile Measurements with a Heavy Ion Beam Probe in the Compact Helical System; Sep. 1996 (IAEA-CN-64/C1-5)

NIFS-445 O. Motojima, N. Yanagi, S. Imagawa, K. Takahata, S. Yamada, A. Iwamoto, H. Chikaraishi, S. Kitagawa, R. Maekawa, S. Masuzaki, T. Mito, T. Morisaki, A. Nishimura, S. Sakakibara, S. Satoh, T. Satow, H. Tamura, S. Tanahashi, K. Watanabe, S. Yamaguchi, J. Yamamoto, M.Fujiwara and A. Iiyoshi,
Superconducting Magnet Design and Construction of LHD; Sep. 1996 (IAEA-CN-64/G2-4)

NIFS-446 S. Murakami, N. Nakajima, S. Okamura, M. Okamoto and U. Gasparino,
Orbit Effects of Energetic Particles on the Reachable β–Value and the Radial Electric Field in NBI and ECR Heated Heliotron Plasmas; Sep. 1996 (IAEA-CN-64/CP -6) Sep. 1996

NIFS-447 K. Yamazaki, A. Sagara, O. Motojima, M. Fujiwara, T. Amano, H. Chikaraishi, S. Imagawa, T. Muroga, N. Noda, N. Ohyabu, T. Satow, J.F. Wang, K.Y. Watanabe, J. Yamamoto , H. Yamanishi, A. Kohyama, H. Matsui, O. Mitarai, T. Noda, A.A. Shishkin, S. Tanaka and T. Terai
Design Assessment of Heliotron Reactor; Sep. 1996 (IAEA-CN-64/G1-5)

NIFS-448 M. Ozaki, T. Sato and the Complexity Simulation Group,
Interactions of Convecting Magnetic Loops and Arcades; Sep. 1996

NIFS-449 T. Aoki,
Interpolated Differential Operator (IDO) Scheme for Solving Partial Differential Equations; Sep. 1996

NIFS-450 D. Biskamp and T. Sato,
Partial Reconnection in the Sawtooth Collapse; Sep. 1996

NIFS-451 J. Li, X. Gong, L. Luo, F.X. Yin, N. Noda, B. Wan, W. Xu, X. Gao, F. Yin, J.G. Jiang, Z. Wu., J.Y. Zhao, M. Wu, S. Liu and Y. Han,
Effects of High Z Probe on Plasma Behavior in HT-6M Tokamak; Sep. 1996

NIFS-452 N. Nakajima, K. Ichiguchi, M. Okamoto and R.L. Dewar,
Ballooning Modes in Heliotrons/Torsatrons; Sep. 1996 (IAEA-CN-64/D3-6)

NIFS-453 A. Iiyoshi,
Overview of Helical Systems; Sep. 1996 (IAEA-CN-64/O1-7)

NIFS-454 S. Saito, Y. Nomura, K. Hirose and Y.H. Ichikawa,
Separatrix Reconnection and Periodic Orbit Annihilation in the Harper Map; Oct. 1996

NIFS-455 K. Ichiguchi, N. Nakajima and M. Okamoto,
Topics on MHD Equilibrium and Stability in Heliotron / Torsatron; Oct. 1996

NIFS-456 G. Kawahara, S. Kida, M. Tanaka and S. Yanase,
Wrap, Tilt and Stretch of Vorticity Lines around a Strong Straight Vortex Tube in a Simple Shear Flow; Oct. 1996

NIFS-457 K. Itoh. S.- I. Itoh, A. Fukuyama and M. Yagi,
Turbulent Transport and Structural Transition in Confined Plasmas; Oct. 1996

NIFS-458 A. Kageyama and T. Sato,
Generation Mechanism of a Dipole Field by a Magnetohydrodynamic Dynamo; Oct. 1996

NIFS-459 K. Araki, J. Mizushima and S. Yanase,
The Non-axisymmetric Instability of the Wide-Gap Spherical Couette Flow; Oct. 1996

NIFS-460 Y. Hamada, A. Fujisawa, H. Iguchi, A. Nishizawa and Y. Kawasumi,
A Tandem Parallel Plate Analyzer; Nov. 1996

NIFS-461 Y. Hamada. A. Nishizawa, Y. Kawasumi, A. Fujisawa, K. Narihara, K. Ida, A. Ejiri, S. Ohdachi, K. Kawahata. K. Toi, K. Sato, T. Seki, H. Iguchi, K. Adachi, S. Hidekuma, S.Hirokura, K. Iwasaki, T. Ido, M. Kojima, J. Koong, R. Kumazawa, H. Kuramoto, T. Minami, I. Nomura, H. Sakakita, M. Sasao, K.N. Sato, T. Tsuzuki, J. Xu, I. Yamada and T. Watari,
Density Fluctuation in JIPP T-IIU Tokamak Plasmas Measured by a Heavy Ion Beam Probe; Nov. 1996

NIFS-462 N. Katsuragawa, H. Hojo and A. Mase,
Simulation Study on Cross Polarization Scattering of Ultrashort-Pulse Electromagnetic Waves; Nov. 1996

NIFS-463 V. Voitsenya, V. Konovalov, O. Motojima. K. Narihara, M. Becker and B. Schunke,

Evaluations of Different Metals for Manufacturing Mirrors of Thomson Scattering System for the LHD Divertor Plasma; Nov. 1996

NIFS-464 M. Pereyaslavets, M. Sato, T. Shimozuma, Y. Takita, H. Idei, S. Kubo, K. Ohkubo and K. Hayashi,
Development and Simulation of RF Components for High Power Millimeter Wave Gyrotrons; Nov. 1997

NIFS-465 V.S. Voitsenya, S. Masuzaki, O. Motojima, N. Noda and N. Ohyabu,
On the Use of CX Atom Analyzer for Study Characteristics of Ion Component in a LHD Divertor Plasma; Dec. 1996

NIFS-466 H. Miura and S. Kida,
Identification of Tubular Vortices in Complex Flows; Dec. 1996

NIFS-467 Y. Takeiri, Y. Oka, M. Osakabe, K. Tsumori, O. Kaneko, T. Takanashi, E. Asano, T. Kawamoto, R. Akiyama and T. Kuroda,
Suppression of Accelerated Electrons in a High-current Large Negative Ion Source; Dec. 1996

NIFS-468 A. Sagara, Y. Hasegawa, K. Tsuzuki, N. Inoue, H. Suzuki, T. Morisaki, N. Noda, O. Motojima, S. Okamura, K. Matsuoka, R. Akiyama, K. Ida, H. Idei, K. Iwasaki, S. Kubo, T. Minami, S. Morita, K. Narihara, T. Ozaki, K. Sato, C. Takahashi, K. Tanaka, K. Toi and I. Yamada,
Real Time Boronization Experiments in CHS and Scaling for LHD; Dec. 1996

NIFS-469 V.L. Vdovin, T.Watari and A. Fukuyama,
3D Maxwell-Vlasov Boundary Value Problem Solution in Stellarator Geometry in Ion Cyclotron Frequency Range (final report); Dec. 1996

NIFS-470 N. Nakajima, M. Yokoyama, M. Okamoto and J. Nührenberg,
Optimization of M=2 Stellarator; Dec. 1996

NIFS-471 A. Fujisawa, H. Iguchi, S. Lee and Y. Hamada,
Effects of Horizontal Injection Angle Displacements on Energy Measurements with Parallel Plate Energy Analyzer; Dec. 1996

NIFS-472 R. Kanno, N. Nakajima, H. Sugama, M. Okamoto and Y. Ogawa,
Effects of Finite-β and Radial Electric Fields on Neoclassical Transport in the Large Helical Device; Jan. 1997

NIFS-473 S. Murakami, N. Nakajima, U. Gasparino and M. Okamoto,
Simulation Study of Radial Electric Field in CHS and LHD; Jan. 1997

NIFS-474 K. Ohkubo, S. Kubo, H. Idei, M. Sato, T. Shimozuma and Y. Takita,
Coupling of Tilting Gaussian Beam with Hybrid Mode in the Corrugated Waveguide; Jan. 1997